Published in final edited form as:
J Phys Chem B. 2013 October 3; 117(39): 11732–11742. doi:10.1021/jp406001b.

Spherical Monovalent Ions at Aqueous Liquid-Vapor Interfaces: Interfacial Stability and Induced Interface Fluctuations

Shuching Ou,
Department of Chemistry and Biochemistry, University of Delaware, Newark, Delaware 19716, USA

Yuan Hu,
Department of Chemistry and Biochemistry, University of Delaware, Newark, Delaware 19716, USA

Sandeep Patel*, and
Department of Chemistry and Biochemistry, University of Delaware, Newark, Delaware 19716, USA

Hongbin Wan
Department of Chemical and Biomolecular Engineering, University of Delaware, Newark, Delaware 19716, USA

Abstract

Ion-specific interfacial behaviors of monovalent halides impact processes such as protein denaturation, interfacial stability, surface tension modulation, and as such, their molecular and thermodynamic underpinnings garner much attention. We use molecular dynamics simulations of monovalent anions in water to explore effects on distant interfaces. We observe long-ranged ion-induced perturbations of the aqueous environment as suggested by experiment and theory. Surface stable ions, characterized as such by minima in potentials of mean force computed using umbrella sampling MD simulations, induce larger interfacial fluctuations compared to non-surface active species, conferring more entropy approaching the interface. Smaller anions and cations show no interfacial potential of mean force minima. The difference is traced to hydration shell properties of the anions, and the coupling of these shells with distant solvent. The effects correlate with the positions of the anions in the Hofmeister series (acknowledging variations in force field ability to recapitulate essential underlying physics), suggesting how differences in induced, non-local perturbations of interfaces may be related to different specific-ion effects in dilute biophysical and nanomaterial systems.

*Corresponding author. sapatel@udel.edu.

Supporting Information Available

Supporting Information Available Supporting Information discusses fluctuation profiles for all ions studied in this work. Further details of entropy calculations are also provided. Comparison of PMF's obtained using umbrella sampling with WHAM and Adaptive Biasing Force method are shown. Uncertainty in PMF calculations are also discussed. Sample input script for NAMD calculation is also provided. This information is available free of charge via the Internet at http://pubs.acs.org.

Keywords

ions; liquid-vapor interface; surface-stability; Hofmeister; fluctuations

I. INTRODUCTION

Molecular and atomic origins of the numerous physical effects induced by the addition of solutes and co-solutes to aqueous environments continue to garner tremendous scientific attention; in particular, questions about the driving forces for such processes, (free) energetic and entropic underpinnings of these effects, and general, quantitative models are actively pursued. A short list of relevant issues includes protein denaturation and folding in aqueous solutions by co-solutes[1,2], Hofmeister effects related to modulation of surface tension and protein solubility[3-5], anion-specific interfacial stability[6-10] as suggested by ambient pressure x-ray photoelectron spectroscopy (XPS), vibrational sum frequency generation (VSFG), and second-harmonic generation (SHG) studies of liquid-vapor (L-V) interfaces of aqueous halide solutions, and differential cation influences on multi-walled carbon nanomaterial aggregation kinetics[11]. In these contexts, the role of the interface, defined loosely as the boundary between water and any relevant (bio)molecular species, is critical. Moreover, the response of the water-(bio)molecule interface to added impurities would be central to such effects. Furthermore, one may ask about how the impurity might influence the behavior of the interface from afar? Is there a plausible interpretation? We bring to attention recent studies suggesting that ions modulate hydration water structure and properties over large distances[12-19]; even large macromolecules have been shown to induce dramatically long-ranged perturbations of water dynamics[20]. First hydration shell water molecules may not provide a complete picture in terms of understanding the above-mentioned physical behaviors in a holistic manner. Acknowledging long-range perturbations by impurities, one must connect such perturbations to observed physical phenomena. Here we attempt to provide a connection between local ion hydration, long-range perturbations, and surface stability of Hofmeister series anions, acknowledging that this is one specific context. In this work, we stress that we are not commenting on the accuracy of any of these force fields, as all water-ion force field combinations have been carefully parameterized and validated via extensive structural and thermodynamic analysis elsewhere. We are interested in extracting underlying behaviors that possibly help to discern between species exhibiting interfacial stability and those that do not. To achieve this, in the context of spherical, monovalent ion thermodynamics at aqueous liquid-vapor interfaces, we will apply classical molecular dynamics simulations using a set of different non-additive and additive intermolecular potential functions to compute the reversible work of moving an ion from bulk to vapor through the interface; we will also extract from these all-atom simulations fluctuations of the liquid-vapor interface, and specifically, the manner in which the ions and their complex hydration shells couple with solvent to give rise to interfacial fluctuations. The connection between differences in induced interface fluctuations and differences in solvation environment of a series of monovalent ions is a novel finding of this work. In Section II A we will discuss the methods, force fields, and other analysis protocols. In Section II C, we briefly present our analysis of instantaneous interfaces and their fluctuations as extracted from all-atom molecular dynamics simulations (following a method developed by Willard

and Chandler[21]), and in Section III we will present our results of potentials of mean force for a variety of ions modeled with polarizable and non-polarizable force fields, interface fluctuations and how each ion affects these, and finally connecting the nature of hydration shells of the series of ions to the trends in surface / interface stability demonstrated by the potentials of mean force.

II. METHODS

A. Simulation Details

In this study we used one nonpolarizable force field as well as three different polarizable force fields. We will first introduce the common simulation protocol, then describe them in detail. Molecular dynamics simulations were performed using the CHARMM package[22] (for SPC/E, TIP4P-FQ and TIP4P-QDP) and the parallel, scalable MD program NAMD 2.9b3[23] (for SWM4-NDP). Simulations of liquid-vapor interfaces were performed in the *NVT* ensemble. Temperature was maintained at T = 300 K using Nosé-Hoover thermostat[24] for SPC/E, TIP4P-FQ and TIP4P-QDP, while Langevin friction force scheme was used in NAMD with the damping coefficient = 5ps^{-1} for SWM4-NDP. The simulation cell was rectangular with dimensions 24 Å × 24 Å × 100 Å, in which z is the direction normal to the liquid-vapor interface. Periodic boundary conditions were applied in all three spatial directions. A bulk slab consisting of 988 water molecules (represented by the nonpolarizable SPC/E model[25] as well as the polarizable TIP4P-FQ model[26], TIP4P-QDP[27,28], or SWM4-NDP[29]) and a single ion (F^-, Cl^-, Br^-, I^-, Na^+, K^+, Cs^+) was positioned in the center of the simulation cell, resulting in two liquid-vapor interfaces. A rigid water geometry is enforced using SHAKE[30] constraints. Before the production simulations, the system of each window was equilibrated for at least 0.5 ns.

1. TIP4P-FQ and TIP4P-QDP—We employ polarizable TIP4P-FQ[26] and TIP4P-QDP[28,31] water models and non-polarizable ions treated as charged Lennard-Jones spheres. Polarization of water is treated with a charge equilibration Hamiltonian[32-35]:

$$E_{elec}=\sum_{i=1}^{N}(\mathscr{X}_i)\,q_i+\frac{1}{2}\sum_{i=1}^{N}\eta_i q_i^2+\frac{1}{2}\sum_{i\neq j}^{N}J_{ij}q_iq_j \quad (1)$$

where $\mathscr{X}_i$ and η_i may be associated with atomic electronegativities and hardnesses, respectively; the J_{ij} terms represent a parameterized molecular Coulomb integral between pairs of atoms. Components of the molecular polarizability tensor are related to the inverse of the hardness matrix (constructed from the values of η_i and J_{ij} above) as $\alpha_{\beta_\gamma} = \mathbf{R}_\beta\,\mathbf{J}^{-1}\,\mathbf{R}_\gamma$ where $\mathbf{R}_\beta$ represents the β Cartesian components of the atomic position vector[36].

Both water models employ a rigid geometry having an O-H bond distance of 0.9572 Å, an H-O-H bond angle of 104.52° and a massless, off-atom *M* site located 0.15 Å along the H-O-H bisector which carries the oxygen partial charge. Repulsion and dispersion interactions are modeled using a single Lennard-Jones (LJ) site located on the oxygen center having parameters $R_{min,O}$ = 3.5459 Å and ε_O = 0.2862 kcal mol^{-1} for TIP4P-FQ, $R_{min,O}$ = 3.5606 Å and ε_O = 0.3501 kcal mol^{-1}, respectively.

Ions were treated as non-polarizable particles with interaction parameters based on those by Lamoureux and Roux[37] and validated for use with TIP4P-FQ[38-42]. For ions in TIP4P-QDP, the parameters were obtained from Reference[42]. Ion parameters in SPC/E were parameterized by Fyta et al[43,44]. We acknowledge that the use of a mixed polarizable water model with non-polarizable anion representation may appear unorthodox, but we consider that the combination of this *empirical* model is well-validated and reproduces many of the currently-accepted experimental observables upon which the quality of such force fields are based. Furthermore, the use of an alternative force field model allows us to speak to the universality (or at least the broad commonality) of molecular and atomic features underlying observed behaviors such as surface stability and negative surface adsorption entropy.

We summarize the parameters used in Table II. The non-bond interactions were treated via the standard Lennard-Jones "12-6" potential

$$E_{LJ}=\sum_{ij}\varepsilon_{ij}\left(\frac{R_{min,ij}^{12}}{r_{ij}^{12}}-2\frac{R_{min,ij}^{6}}{r_{ij}^{6}}\right) \quad (2)$$

Lennard-Jones interactions were gradually switched off at interparticle distance of 11 Å, with a gradual switching between 10 Å and 11 Å using the switching function:

$$S\left(r_{ij}\right)=\begin{cases}1 & r_{ij}\leq r_{on}\\ \frac{\left(r_{off}^2-r_{ij}^2\right)^2\left(r_{off}^2+2r_{ij}^2-3r_{on}^2\right)}{\left(r_{off}^2-r_{on}^2\right)^3} & r_{on}<r_{ij}\leq r_{off}\\ 0 & r_{ij}>r_{off}\end{cases} \quad (3)$$

Charge degrees of freedom for the TIP4P-FQ and TIP4P-QDP water models were coupled to a thermostat at 1K with mass 0.000069 kcal mol^{-1} ps^2 e^{-2} using the Nosé-Hoover method and the charge degrees of freedom were propagated in an extended Lagrangian formalism; each water molecule was taken as a charge normalization unit (charge conserved with this unit), thus preventing any charge transfer between water molecules or between water and ion. We acknowledge recent developments of charge transfer models of water[45,46], and anticipate that application of charge transfer models to the study of specific-ion effects will soon be realized and further elucidate underlying mechanisms and physics. Conditionally convergent long-range electrostatic interactions were treated using Particle Mesh Ewald (PME)[47] approach with a 30×30×128 point grid, 6th order interpolation, and $\kappa = 0.33$. Dynamics were propagated using a Verlet leap-frog integrator with a 0.5 fs timestep for TIP4P-FQ and TIP4P-QDP, 1 fs timestep for SPC/E. Total sampling time for each window was 5-20 ns; properties were calculated from all but the initial 0.5 nanosecond, which was treated as equilibration.

2. SWM4-NDP—Associated with the explicit SWM4-NDP water force field, ions were also represented with a Drude oscillator model as discussed in Reference[48]. The parameters were obtained from Reference[48]. A timestep of 1.0 fs was used to integrate the equations of motion. Particle Mesh Ewald (PME) was implemented to treat conditionally convergent long-range electrostatic interactions(using a grid of 32 × 32 × 128 points. The cutoff for van

der Waals (VDW) interactions was set to 15 Å without smoothing functions. An analytical correction of Lennard-Jones was applied to the reported vdW energy and virial that is equal to the amount lost due to cutoff of the LJ potential. The temperature was kept constant by applying the Langevin friction force scheme ($5ps^{-1}$ was used for the damping coefficient). The long-range Coulombic forces were updated every two steps. The van der Waals interactions were modified using scale 1-3 parameters defined in the NAMD protocol and truncated smoothly at the cutoff distance. To ensure near-SCF conditions, the thermostat for the relative motion of the Drude particles with respect to their parent atoms was set at a temperature of 1 K with a damping coefficient of 20 ps^{-1}. The rigid geometry of the SWM4-NDP water molecule was maintained using the SETTLE algorithm[49]. An additional quartic restraining potential of 4000 kcal/mol/$Å^2$, fitted from QM calculations, was applied to a Drude oscillator if its length exceeded 0.2 Å (fitted from QM calculations). These technical details are implemented in NAMD2.9 and were used without modification in the current work. A NAMD input file for the Drude oscillator ABF simulation for sodium cation in SWM4-NDP water is provided at the end of Supporting Information.

B. Potential of Mean Force Calculation

We will present potential of mean force (PMF) results for the reversible work of transferring ions from bulk solution through the liquid-vapor interface, to the vapor phase. The PMF will characterize the interfacial stability of each ion. Computational experiments measuring the reversible work (potential of mean force, PMF) for transferring single ions/molecules from bulk aqueous environment to the aqueous solution liquid-vapor interface have enjoyed a long history as a means to explore the origins of surface stability[50-52]. For potential of mean force calculations of SPC/E, TIP4P-FQ and TIP4P-QDP, our reaction coordinate, ξ_0, is the Cartesian z-component of the separation between the water slab center of mass and ion center of mass. In all simulations used for computing potentials of mean force, ions were restrained to z-positions from 10 Å to 35 Å relative to the water slab center of mass using a harmonic potential $\mathrm{U}_{restraint}\left(z;z_{relative,ref}\right)=\frac{1}{2}k_{restraint}\left(z-z_{relative,ref}\right)^2$ with the force constant of 4 (kcal/mol)/$Å^2$; this encompasses a range approximately 15 Å below the Gibbs Dividing Surface (GDS) to approximately 10 Å above it at 300 K; though one could probe separations further into the bulk (towards the center of the system) this distance is sufficient to probe the differences of interest in this study, and also in keeping with previous studies to which we compare our results. We note the recent connection of the potential of mean force to thermodynamic free energies[53]:

$$\begin{aligned}\frac{dA(\xi_0)}{d\xi_0} &= \left\langle \left(\frac{\partial U_{interaction}(\mathbf{r}^N)}{\partial q_\xi} \right)_{\{q_{m\neq\xi}\}^{N-1}} \right\rangle_{\xi_0} - \left\langle \frac{1}{\beta} \left(\frac{\partial \ln |J|}{\partial \xi} \right)_{\{q_{m\neq\xi}\}^{N-1}} \right\rangle_{\xi_0} \\ &\quad - \frac{1}{\beta} \left\langle \sum_{m\neq\xi}^{N-1} \left[\delta\left(q_m - l_{U_m}\right) \frac{dl_{U_m}(q_m)}{dq\xi} - \delta\left(q_m - l_{L_m}\right) \frac{dl_{L_m}(q_m)}{dq\xi} \right] \right\rangle_{\xi_0}\end{aligned} \quad (4)$$

where the interaction potential is taken to be a function of some set, of the size of the number of system degrees of freedom, of generalized coordinates, q_ξ. The reaction coordinate of interest in this case corresponds to $q_\xi = \xi_0$.

The first term is the negative of the mean force whose integral over the domain of the reaction coordinate yields the potential of mean force. The second term arises from the volume scaling upon transforming from Cartesian to some generalized curvilinear space (represented in general by the set of generalized coordinates). The last term arises from interchange of the order of the differential and integral operators according to Leibniz rule. In the present study, as we retain the Cartesian z-component of the separation between centers of mass (the force is projected along this reaction coordinate), and the domain of the reaction coordinate is decoupled from those of the remaining coordinates (the derivatives in the Leibniz term are zero), the Jacobian and Leibniz terms vanish. Thus we discuss the PMF in terms of the free energy or reversible work for the remainder of the paper.

The free energy profiles in SWM4-NDP force field were performed by using NAMD software with the Adaptive Biasing Force (ABF) extensions integrated in the Collective Variables module and under the same conditions as described for MD simulations. Thirty-two "windows" along positive z–direction were explored, each with 1.5 Å width. Force samples were accumulated in bins 0.02 Å. [−1.5-00.5], [00-01.5], [01-02.5], [02-03.5], [03-04.5], [04-05.5], [05-06.5], [06-07.5], [07-08.5], [08-09.5], [09-10.5], [10-11.5], [11-12.5], [12-13.5], [13-14.5], [14-15.5], [15-16.5], [16-17.5], [17-18.5], [18-19.5], [19-20.5], [20-21.5], [21-22.5], [22-23.5], [23-24.5], [24-25.5], [25-26.5], [26-27.5], [27-28.5], [28-29.5], [29-30.5], [30-31.5].

The uncertainties in potentials of mean force are determined using the approach of Zhu and Hummer[54]:

$$var\left[G\left(\xi_{N}\right)\right] \approx \sum_{i=1}^{N} var\left[K\Delta\xi\bar{z}_{i}\right] \quad (5)$$

where $\bar{z}_i$ is the mean position of z in the i_{th} window, which can be obtained from block averages[55]. K is the force constant. The corresponding standard deviation $\sigma[G(\xi_N)]$ is then the square root of var$[G(\xi_N)]$. In our case, $G(z_{bulk}) = 0$, therefore the last window is expected to have the largest uncertainty. The largest uncertainties for the systems are approximately 0.1 kcal/mol (shown in Figure 1 of Supporting Information). Alternative measures of estimating the mean and uncertainty of other properties will be discussed as needed.

C. Instantaneous Interfaces and Surface Fluctuations

For an instantaneous surface snapshot, the local density profile can be defined as[56]:

$$\left\langle \rho\left(\vec{r}_{xy}, z\right)\right\rangle \equiv \frac{1}{A_{\xi}} \int d^{2}\vec{r}'_{xy} \rho\left(\vec{r}_{xy} - \vec{r}'_{xy}, z\right) = \rho\left[z - h\left(\vec{r}_{xy}\right)\right] \quad (6)$$

which describes the short-distance average of the density over an area $A_\xi \sim \xi^2$ at position $\vec{r}_{xy}$. ξ is an inherent correlation length. Here we define $\delta h\left(\vec{r}_{xy}\right) = h\left(\vec{r}_{xy}\right) - z$ as surface height function. Notice that under this definition we have $\left\langle \delta h\left(\vec{r}_{xy}\right)\right\rangle = 0$.

From individual snapshot/configuration we can construct the coarse-grained instantaneous surface defined by Willard and Chandler[57]. Gaussian mass distributions are assigned to each water oxygen atom:

$$\Phi(\mathbf{r};\xi) = \left(2\pi\xi^2\right)^{-d/2} exp\left(-r^2/2\xi^2\right) \quad (7)$$

where r is the magnitude of $\mathbf{r}$, ξ is taken as 3.0 Å, and d stands for dimensionality (3 in this case). At space-time point $\mathbf{r}$, t, we have the coarse-grained density as

$$\bar{\rho}(\mathbf{r},t) = \sum_j \Phi(|\mathbf{r} - \mathbf{r}_i(t)|;\xi) \quad (8)$$

The interface is then determined as the $(d - 1)$-dimensional manifold with a constant value c. In practice, we set up series of spacial grid points (x, y, z) and compute the corresponding coarse-grained densities $\rho(x, y, z)$ by Equation 8.[58] The resolution we use for x and y dimensions is 0.6 Å between grid points; for z dimension the grid resolution is 0.1 Å. The surface is then obtained as the manifold by setting $\rho(x, y, z) = \rho_{bulk}/2$. With sufficient sampling, we can average these instantaneous surfaces ($h_t(x, y)$, at time t) and get the mean surface $\mathrm{h}h(x, y)\mathrm{i}$; furthermore, $\langle \delta h(x, y) \rangle = 0$. Subtracting the mean values from the $h_t(x, y)$, we obtain $\delta h_t(x, y)$ and the height fluctuations $\delta h_t^2(x, y)$. Using this framework to characterize interface fluctuations, we can probe the magnitudes of interface fluctuations when the ions reside at various positions along the reaction coordinate.

III. RESULTS AND DISCUSSION

A. Potential of Mean Force and Surface Fluctuation

We begin by looking at the free energetics of ions across the liquid-vapor interface. This will show which of the model ions (in their respective types of solvent) are predicted to be interface stable, and to what extent as indicated by the magnitude of the PMF well-depth at the interface. In all cases, the position of the Gibbs dividing surface (GDS) is around z = 25.6 Å; since the GDS is determined predominantly by the water density, the presence of a single ion of varying size does not influence to any large extent the less-resolved GDS across all systems. Figure 1 shows the potential of mean force (PMF) of single anion/cation in different force fields (K^+ is shown in Figure 2 of Supporting Information). For clarity, we added a vertical off set of 2 kcal/mol between each force field. As a reminder, for SPC/E, TIP4P-FQ and TIP4P-QDP we used umbrella sampling in conjunction with WHAM[59] to compute the PMF; for SWM4-NDP we used ABF. The PMF is defined to be zero in the bulk (which is determined by window z = 10 Å). The PMF from ABF method is consistent with the umbrella sampling method, which is verified in Supporting Information, Figure 11. All the cations and F^- shows no PMF minimum regardless of force field. For Cl^-, the TIP4P-QDP force field shows modest surface stability; in SWM4-NDP there is a barrier observed around z = 21 Å, followed by a shallow minimum after the barrier. We observed PMF minima for Br^- in polarizable force fields but no surface stability in nonpolarizable force fields. Br^- has been considered marginally surface stable so the greatest effect of polarization may be expected to occur with this ion (i.e, surface stability systematically

emerging with the introduction of ion polarizability). For I^-, PMF minima are observed in all force fields with the sequence $G_{SWM4–NDP} < G_{TIP4P–QDP} < G_{TIP4P–FQ} \approx G_{SPC/E}$. The results for Drude I^- are consistent with the surface stability discussed by Archontis et al[60]. Incidentally, at 300 K, I^- shows a minimum of 0.5 kcal/mol in TIP4P-FQ, which is similar to the result for iodide at the L-V interface using non-polarizable ions in SPC/E water by Horinek et al[61,62]. This also corresponds with the DFT-D value determined by Baer *et al*[63], though we do not discount that ours is a fortuitous result to some degree. In our simulation, we do not include explicitly the polarization of the I^-, but we have taken care to faithfully capture the relative hydration free energetics of the individual ions to as great an extent as possible. Though not possible currently, it would be interesting to connect the hydration free energetics of ions using DFT-D methods in order to further assess and characterize such agreements between classical models and electron-density based models

Recent studies have demonstrated a connection between L-V interfacial stability of chemical species (i.e. a free energy minimum state with the solute at the interface) and the extent to which the presence of these molecular species in the vicinity of the interface induces collective fluctuations of the interface in addition to the level inherent in pure water due to thermal motion[6,58]. In the next discussion, we explore the differences in interfacial fluctuations for the various ions discussed in this study. We aim to further demonstrate the general connection between interfacial stability and fluctuations with different force fields.

Figure 2 shows the fluctuations $\langle \delta h^2(x, y) \rangle$ for I^- at different restrained *z*-position in TIP4P-FQ force field. When the anion is in the bulk (i.e. $z = 10$ Å), $\langle \delta h^2(x, y) \rangle$ is about 0.56, which corresponds to the value of pure TIP4P-FQ (refer to Ref[58]); at $z = 18.0$ Å, we observe onset of enhanced fluctuations relative to the pure water system. This enhancement reaches a maximum while I^- is restrained at $z = 21$ Å (as shown in Figure 2b). Finally when the anion moves across the GDS ($z = 25$ Å), the interfacial fluctuation is suppressed (as shown in Figure 2c). To illustrate this feature, we plot $\langle \delta h^2(x = 0, y = 0) \rangle$ as a function of the anion restrained *z*-position, as presented in Figure 2d.

From Figure 2b and c we can see that the geometry of the $\langle \delta h^2(x, y) \rangle$ surface possesses radial symmetry and can thus be presented as a function of the lateral distance $r = \sqrt{x^2 + y^2}$ the case of pure water (in the absence of ions), $\langle \delta h^2 \rangle$ for the current system size for the current force fields are 0.62 (SPC/E), 0.56 (TIP4P-FQ), 0.52 (SWM4-NDP) and 0.58 (TIP4P-QDP). Therefore, in order to demonstrate and compare the fluctuations induced from the ions, we define $\delta h_L^2(r)$ as the fluctuations normalized by the value of pure water fluctuation in the corresponding force field. In this convention, when $\langle \delta h_L^2 \rangle$ equals 1, the effect of ion is zero; when $\langle \delta h_L^2 \rangle > 1$, the surface height fluctuation is enhanced relative to pure water with the presence of ion; when $\langle \delta h_L^2 \rangle < 1$, the surface height fluctuation is suppressed. Here we would like to address that, although the surface fluctuation of pure water for the same force field does change according to the size of the simulation cell (basically, the larger the *x, y* dimensions, the larger the fluctuation value), the normalized $\langle \delta h_L^2 \rangle$ remains the same for the same ion at the same relative position along the reaction

coordinate, which indicates that the ion-induced fluctuation is indeed a characteristic of the ion and is system size independent (data shown in Supporting Information, Figure 4).

Figure 3 shows the $\left\langle \delta h_{\mathrm{L}}^{2}\,(r) \right\rangle$ from I^- (surface stable in all force fields) and Na^+ (non-surface stable), at the restrained window which induces the largest possible surface fluctuation and GDS. Fluctuation profiles for other ions can be found in Supporting Information, Figures 5 through 10). Here we chose these two species to describe the general properties and connection between surface stability and surface height fluctuation. First, either anion or cation suppresses the fluctuation when the ion is at the GDS, which is consistent with previous studies[6,58,64]. Na^+ does not generate any fluctuation enhancement. Only the surface stable species, I^-, induces interfacial fluctuation, in fact up to two times the inherent fluctuation from pure water. This fluctuation enhancement can influence the interface up to 8 Å from the ion center. Furthermore, at $r = 0$ Å (which indicates right above/below the ion), we have $\left\langle \delta h_{L,SWM4-NDP}^{2} \right\rangle > \left\langle \delta h_{L,TIP4P-QDP}^{2} \right\rangle > \left\langle \delta h_{L,TIP4P-FQ}^{2} \right\rangle \approx \left\langle \delta h_{L,SPC/E}^{2} \right\rangle$. This is the opposite sequence of the corresponding ΔG values. We also notice that from Figure 2d, which plots values of $\left\langle \delta h_{\mathrm{L}}^{2}\,(r{=}0) \right\rangle$ as a function of ion position along the interface normal from bulk to GDS, (and Figure 7 of Ref[58]), though Cl^- in TIP4P-FQ induces less enhancement of fluctuations (about half of I^--induced), yet we still find no surface stability for Cl^- in TIP4P-FQ water. This suggests a threshold level of induced fluctuations separating surface-stable ions; this would be ion-specific and the precise value for a particular ion-water force field would be determined by the complex interplay of water-water, ion-water interactions, and how these vary with proximity to the ion (i.e, nature of hydration shell of the ion in a particular solvent force field model as we will discuss further below). Furthermore, we have demonstrated that for species such as Cl^- in TIP4P-FQ water, there is no temperature-dependent variation of $\delta h^2_{\mathrm{L}}(r)$, opposite to what is observed for I^-; we interpret this to mean that there is no real interfacial enhancement from the non surface-stable ion. This is rationalized by the fact that with increasing temperature, the increased inherent thermal fluctuations of the water interface wash out any induced fluctuations arising from perturbation of solvent structure by the ion[58].

To summarize up to this point, we have found that across a variety of force fields for ions and solvent, there is a group of ions that exhibit interfacial stability as seen in the potentials of mean force. In this work, we stress that we are not commenting on the accuracy of any of these force fields, as all water-ion force field combinations have been carefully parameterized and validated via extensive structural and thermodynamic analysis elsewhere. We have then seen that the species demonstrating an interfacial stability appear to enhance liquid-vapor interfacial fluctuations significantly, while those that show no interfacial stability induce no further fluctuation (or may even suppress levels of fluctuations). Our analysis further suggests the existence of inherent levels of fluctuation that correspond to interfacial stability that are force field specific, and arise from complex interactions of the models. Figure 4 shows results of the PMF value at the position of the GDS versus the maximum interfacial fluctuations induced. This is a plot that only distinguishes between ions; the different water force fields are not isolated. We see that the ions displaying interface stability lie in the upper left quadrant of the figure; those showing no stability

(positive values of PMF) reside in the lower right quadrant. A best-fit straight line indicates a threshold value of about 1.5 dividing those ions that are interfacially stable and those that are not. The value of 1.5 is not an absolute threshold; this will depend on the force field (as noted above), size of the interfacial area, and is sensitive to the parameters of the protocol (width of Gaussian for coarse-graining water density) used to compute instantaneous interfaces and fluctuations. Nevertheless, the qualitative behavior and results should be robust.

We will next attempt to explain the current observations by considering the interaction of the local hydration environment of the ions with the solvent and solvent fluctuations at the L-V interface. We aim to show that the two types of ions (surface stable and unstable) present distinct hydration shell environments towards the interface upon approach; the surface stable ions presenting a solvent environment that is less rigid, more malleable, and thus more amenable to inducing fluctuations of the interface as a consequence of a greater disruption of solvent structure on approach to the interface. The non surface-stable ions present a more rigid hydration environment due to the more effective hydrogen bonding of water, thus decreasing the efficacy of promoting interfacial fluctuations. These properties of the two orientations are discussed using radial density profiles of water around the single ions and water velocity autocorrelation functions in the hydration shells presented to the interface in the vicinity of the GDS.

B. Solvation Structure and Dynamical Properties

We first consider general characteristics of ion hydration through radial density functions (RDF's)shown in Figure 5. In panels a,b,c, and d we show results for anions and cations (in insets) in the various water models (on F^- ion model has been developed for the TIP4P-QDP water force field currently). Regardless of water force field or inclusion of polarizability, there is a general trend from F^- to I^- of decreasing water structuring around the anion (similarly for the cation series from Na^+ to Cs^+). The more severe ordering of water molecules around Cl^- is well-known[65,66]. Smaller anions show dramatic first solvation peaks, and a sharply oscillatory probability function; in contrast, the larger anions show modest peaks, and significantly less oscillations. Figures 6a, b, and c a show the 360° angle-averaged radial water density around I^-, Cl^-, and Na^+ as they reside at z=21.0 Å, the position of maximum $< \delta h^2_X(x, y) >$ for the anions (the cation shows no maximum, but we use the same distance for all ions for consistency). This Figure demonstrates the different manners in which the hydration shells of the ions couple with the solvent at the interface. I^-, while retaining its first, weakly-bound, less-ordered (malleable) hydration shell, sheds its outer hydration layers in the sense that these shells intermingle with the interfacial solvent. Cl^-, in contrast, retains the first and most of the second hydration shells (two bright rings); thus, the hydration shell environment is more rigid, well-ordered, tightly bound to the ion and does not support increased dynamical perturbation of local solvent. Moving to the cation, Na^+, panel c demonstrates the unambiguous, well-defined hydration shells, with a fully intact second shell clearly visible. We conjecture that the differences in water dynamics and structure in the first and second hydration shells of I^- and Cl^- lead to differences in induced interfacial fluctuations. To explore this, we will consider first water (oxygen) velocity autocorrelation functions (vacf's) and residence times of water in the

hydration shells of select ions. Since our contention is based on the nature of the hydration shell environment presented to the interface as the ion approaches, we will consider properties of hydrating water above the ion as depicted in panels d, e, and f of Figure 6. Shown in panels d,e, and f are the mean coarse-grained interfaces when the ions are positioned at z=21Å. These panels further demonstrate how the hydration shells of each ion (boundaries of which are delineated by the dashed circles around each ion) interact with the mean interface and the interfacial region in general. In the case of I^-, it is plausible to entertain the idea that less ordered, dynamic, weakly-bound water in these shells can help induced fluctuations about the mean interface. In the case of the other two ions, the mean interface is further away, and the rigidity of these ions' solvation shells prevents fluctuations that would penetrate into the local hydration shells. We now consider vacf's.

C. Water Velocity Autocorrelation Functions and Residence Times

Ensemble-averaged oxygen velocity autocorrelation functions (VACF)[67-69],

$$C_v(t) = \frac{\langle \overrightarrow{v_i}(t) \cdot \overrightarrow{v_i}(0) \rangle}{\langle \overrightarrow{v_i}(0) \cdot \overrightarrow{v_i}(0) \rangle} \quad (9)$$

where $\overrightarrow{v_i}(t)$ is the velocity vector of the atom (the oxygen in our case) in i_{th} water molecule in the simulation system at time *t*. The brackets denote the ensemble average. Here we only look at the VACF of water oxygen above the ion and within the first/second shell.

Figure 7 shows oxygen-oxygen vacf for I^- and Cl^- in TIP4P-FQ water for three ion positions corresponding to bulk solution (z=10Å), position of maximum fluctuation enhancement (z=21Å), and the GDS (z=25Å). Autocorrelation functions are shown for first hydration shell waters (solid line), second hydration shell waters (dashed line), pure bulk water (open circles), and pure water liquid-vapor interface (open squares). The solid and dashed lines represent correlation functions for water molecules in the regions depicted in Figure 6. We see that the location of the ions influences the dynamics of water in their hydration shells. At the bulk, z=10Å, position, for both anions, autocorrelation functions are bulk-like as expected. We notice the canonical caging effect of local solvent molecules manifest in oscillations around 100fs. At ion position z=21Å, for the I^- system, we see little difference between autocorrelation decay in the first and second hydration shells unlike in the Cl^- system. The shortest time to approach zero is 185 – 190 *fs* for I^-, 160 *fs* for Cl^- in the first shell, and 180 *ps* for Cl^- in the second shell. The shorter decorrelation times for Cl^- are consistent with a higher shell water density. Furthermore, the I^- curve takes a form closer to that of the pure liquid-vapor interface, while the Cl^- curve retains the oscillatory "hump" (though damped) of the bulk liquid curve, particularly the Cl^- first hydration shell. This indicates that the well-known caging effect persists for Cl^-. The local hydration environments for I^- and Cl^- are quite different approaching the interface.

Water residence time is considered a time-dependent probability function $P(t)$ of a molecule uninterruptedly remaining in a region at time $t = t_0 + \Delta t$ having started in the region at time t =0 $P(t) = \frac{1}{N(0)} \Sigma_{t_0} N(t_0, t)$. We consider molecules that are with in the first/second shell at

time $t_0 = 0$ and remain with in the corresponding shell at t with no instances of leaving the region. The probability is $P(t) = \frac{1}{N(0)} \Sigma_{t_0} N(t_0, t)$

$$P(t) = \frac{1}{N(0)} \sum_{t_0} N(t_0, t) \quad (10)$$

where t_0 indicates multiple time origins and $t = t_0 + t$ is the persistence time of a water molecule in a region after it was initially observed at time origin t_0. The number of molecules confined at each time t is normalized by the number of molecules observed at $t = 0$, such that $P(0) = 1$. We employ a 5 fs saving frequency for this analysis. $P(t)$ is fit to a stretched exponential, $P(t) = P_0 exp[-(t/\tau)^{\gamma}]$

$$P(t) = P_0 exp\left[-(t/\tau)^{\gamma}\right] \quad (11)$$

where P_0, τ, and γ are adjustable fitting parameters. P_0 is probability that a water molecule initially is within the shell at time t=0; for the final functional fits, P_0 is approximately 1. γ is the well-known stretched exponential constant and is generally around 0.85, suggesting deviation from first order decay. τ is characteristic residence lifetime. Residence times of water molecules (only those above the ion) residing in the first solvation of I^- and Cl^- are shown in Table III. Data for I^- and Cl^- using TIP4P-FQ and SWM4-NDP water models are shown as representative examples. For all positions, water residence times in the first hydration shell of Cl^- are higher than for I^-. At z=21.0 Å the ratio can reach a striking factor of 2. This suggests that the first hydration shell of Cl^- acts as a barrier to surface deformation, preventing deformation to the extent observed for I^-; moreover the mean surface for Cl^- resides in its second hydration shell. Observed differences in ion-induced interfacial fluctuations thus correlate with the lifetimes of hydration water molecules in a particular ion's local environment, the implication being that faster dynamics (smaller lifetimes) allow more exchange of water in hydration shells, allowing for the ability to accommodate/mediate greater fluctuations.

IV. SUMMARY AND CONCLUSIONS

Our findings indicate a connection between interface stability and induced interfacial fluctuations for a series of anions and cations modeled using molecular dynamics simulations. The behavior, as summarized in Figure 4, appears to span a variety of force fields, and does not discriminate based on inclusion or exclusion of polarization in the force field. For purposes of discussion and to connect to implications of this work for underlying mechanistic explanations of differential anion stability at aqueous liquid-vapor interfaces, or action of protein denaturing osmolytes, we explore semi-quantitatively the relation between interface fluctuations and surface entropy. We stress that the surface/interfacial entropy is just one contribution to the overall system entropy. From the interface height function covariance matrix, $\mathscr{X}(\mathbf{r}_i, \mathbf{r}_j) = \langle \delta h(\mathbf{r}_i)\, \delta h(\mathbf{r}_j) \rangle$, with $\delta h(\mathbf{r}_i) = h(\mathbf{r}_i) - \langle h(\mathbf{r}_i) \rangle$, multivariate statistics gives the entropy as $\delta h(\mathbf{r}_i) = h(\mathbf{r}_i) - \langle h(\mathbf{r}_i) \rangle$ (refer to Supporting Information). Figure 8 (symbols) shows estimates of the resulting interfacial entropy (relative to ion z-position 10.0 Å) at ion positions of 21.0 and 25.0 Å; we stress that these values are

qualitative due to the grid-based approach used. In the barrier region, the entropy from surface fluctuations increases for both ions, with I^- contributing more due to larger fluctuations. We posit that in the case of I^-, this higher interfacial entropy acts in conjunction with other enthalpic (i.e., increase in water-water interactions leading to enthalpic stabilization of the system) contributions to greater stabilize I^- at these locations (z=20.0, 21.0 and 22.0 Å) compared to Cl^-. This translates to higher probability of the I^- being in these positions; once at these locations, the I^- can then proceed to the interfacial region. At the Gibbs Dividing Surface (vertical line, Figure 8), suppression of interface fluctuations by both anions leads to lower surface entropy relative to the bulk state. In the case of I^-, the reduction is slightly higher consistent with the trends in Fig 1. The surface adsorbed state for I^- shows a net decrease in entropy relative to the bulk state; this holds for Cl^- as well. For I^-, this is interpreted as one negative contribution to the standard entropy of adsorption.

In summary, negatively charged ionic impurities, I^- and Cl^-, induce long-ranged solvent perturbations that propagate to an interface when the ions are up to 8 Å away in accord with recent experiments and interpretations suggesting the long-range nature of ion-induced perturbations. Furthermore, we observe chemical specificity (ion-specificity); I^- induces larger interfacial fluctuations than Cl^-. The differences in induced fluctuations are traceable to the nature of the first few hydration shells of the ions. For I^-, the hydration shells consist of water molecules that are more dynamic, less persistent (lower residence times), while the opposite is true for Cl^-. Approaching the liquid-vapor interface, coupling of local solvent with solvent further away leads to differential contributions of surface entropy (arising from the different magnitudes of the interface fluctuations) to the stability of surface-adsorbed states. Long-range perturbations are not only relevant to the bulk, but also to the nature of fluctuations at water-biomacromolecule and water-nanomaterial interfaces.

Addressing implications of this work, we note the striking similarity of hydration properties of the less charge-dense I^- to that of hydrophobic hydration[70]. Analogous to enhanced solvent density fluctuations seen for molecular hydrophobic solutes in water[70], I^- perturbs solvent structure and dynamics (to a greater degree than Cl^-) leading to more fluid, dynamic, and fluctuating solvent structure. Furthermore, our observation regarding the connection between the extent of “rigidity” of the first hydration shell of the impurity and its surface stability is reminiscent of Fig S2 of the Supplementary Information of[6]. Overall, results indicate that ion-specific surface adsorption of inorganic monovalent anions may be discussed in the context of increasing ion hydrophobic character as recently suggested[62,71].

Supplementary Material

Refer to Web version on PubMed Central for supplementary material.

Acknowledgments

The authors acknowledge partial support from the National Institutes of Health (COBRE:5P20RR017716-07) at the University of Delaware, Department of Chemistry and Biochemistry. Computational resources are acknowledged via support from National Institutes of Health (COBRE:P20-RR015588) in the Chemical Engineering Department at the University of Delaware. This work is also partially supported by National Science Foundation CAREER AWARD (MCB-1149802) to S. P. We thank Professor Phillip Geissler and Patrick Shaffer for sharing code for

analysis of interface fluctuations and resulting entropy. We acknowledge N. Patel for fruitful discussions and guidance throughout this work.

References

[1]. Hua L, Zhou R, Thirumalai D, Berne BJ. Urea Denaturation by Stronger Dispersion Interactions with Proteins than Water Implies a 2-Stage Unfolding. Proc. Nat. Aca. Sci. 2008; 105:16928–16933.

[2]. Beauchamp KA, McGibbon R, Lin Y-S, Pande VS. Simple Few-State Models Reveal Hidden Complexity in Protein Folding. Proc. Nat. Aca. Sci. 2012; 109:17807–17813.

[3]. Hofmeister F. About Regularities in the Protein Precipitating Effects of Salts and the Relation of These Effects with the Physiological Behavior of Salts. Arch. Exptl. Pathol. Pharmakol. 1887; 24:247–260.

[4]. Baldwin RL. How Hofmeister Ion Interactions Affect Protein Stability. Biophys. J. 1996; 71:2056–2063. [PubMed: 8889180]

[5]. Pegram LM, Wendor T, Erdmann R, Shkel I, Bellissimo D, Felitsky DJ, Record MT. Why Hofmeister Effects of Many Salts Favor Protein Folding But Not DNA Helix Formation. Proc. Nat. Aca. Sci. 2010; 107:7716–7721.

[6]. Otten DE, Shaffer PR, Geissler PL, Saykally RJ. Elucidating the Mechanism of Selective Ion Adsorption to the Liquid Water Surface. Proc. Nat. Aca. Sci. 2012; 109:701–705.

[7]. Noah-Vanhoucke J, Geissler PL. On the Fluctuations That Drive Small Ions Towards and Away From, Interfaces Between Polar Liquids and Their Vapors. Proc. Nat. Aca. Sci. 2009; 106:15125–15130.

[8]. Ghosal S, Brown MA, Bluhm H, Krisch MJ, Salmeron M, Jungwirth P, Hemminger JC. Ion Partitioning at the Liquid/Vapor Interface of a Multi-component Alkali Halide Solution: A Model for Aqueous Sea Salt Aerosols. J. Phys. Chem. A. 2008; 112:12378–12384. [PubMed: 19006284]

[9]. Ghosal S, Hemminger JC, Bluhm H, Mun BS, Hebenstreit ELD, Ketteler G, Ogletree DF, Requejo FG, Salmeron M. Electron Spectroscopy of Aqueous Solution Interfaces Reveals Surface Enhancement of Halides. Science. 2005; 307:563–566. [PubMed: 15681380]

[10]. Tobias D, Hemminger JC. Getting Specific About Specific Ion Effects. Science. 2008; 319:1197–1198. [PubMed: 18309069]

[11]. Yi P, Chen KL. Influence of Surface Oxidation on the Aggregation and Deposition Kinetics of Multiwalled Carbon Nanotubes in Monovalent and Divalent Electrolytes. Langmuir. 2012; 27:3588–3599. [PubMed: 21355574]

[12]. O'Brien JT, Prell JS, Bush MF, Williams ER. Sulfate Ion Patterns Water at Long Distance. J. Am. Chem. Soc. 2010; 132:8248–8249. [PubMed: 20518523]

[13]. Tielrooij KJ. Cooperativity in Ion Hydration. Science. 2010; 328:1006–1009. [PubMed: 20489020]

[14]. Mancinelli R, Botti A, Bruni F, Ricci MA, Soper AK. Perturbation of Water Structure Due to Monovalent Ions in Solution. Phys. Chem. Chem. Phys. 2007; 9:2959–2967. [PubMed: 17551619]

[15]. Horzmann J, Ludwig R, Geiger A, Paschek D. Pressure and Salt Effects in Simulated Water: Two Sides of the Same Coin. Angew. Chemie Intl. Ed. 2007; 46:8907–8911.

[16]. Paschek D, Ludwig R. Specific Ion Effects on Water Structure and Dynamics Beyond the First Hydration Shell. Angew. Chemie Intl. Ed. 2011; 50:352–353.

[17]. Galamba N. Mapping Structural Perturbations of Water in Ionic Solutions. J. Phys. Chem. B. 2012; 116:5242–5250. [PubMed: 22480309]

[18]. Botti A, Bruni F, Imberti S, Ricci MA, Soper AK. Solvation Shell of H+ Ions in Water. J. Mol. Liquids. 2005; 117:77–81.

[19]. Botti A, Bruni F, Imberti S, Ricci MA, Soper AK. Solvation Shell of OH–Ions in Water. J. Mol. Liquids. 2005; 117:81–84.

[20]. Born B, Kim SJ, Ebbinghaus S, Gruebele M, Havenith M. The Terahertz Dance of Water with the Proteins: The Effect of Protein Flexibility on the Dynamical Hydration Shell of Ubiquitin. Faraday Disc. 2009; 141:161–173.

[21]. Willard AP, Chandler D. The Role of Solvent Fluctuations in Hydrophobic Assembly. J. Phys. Chem. B. 2008; 112:6187–6192. [PubMed: 18229916]

[22]. Brooks BR, Brooks CL III, MacKerell AD Jr. Nilsson L, Petrella RJ, Roux B, Won Y, Archontis G, Bartels C, Boresch S, et al. CHARMM: The Biomolecular Simulation Program. J. Comp. Chem. 2009; 30:1545–1614. [PubMed: 19444816]

[23]. Phillips JC, Braun R, Wang W, Gumbart J, Tajkhorshid E, Villa E, Chipot C, Skeel RD, Kale L, Schulten K. Scalable Molecular Dynamics with NAMD. J. Comp. Chem. 2005; 26:1781–1802. [PubMed: 16222654]

[24]. Nosé S. A Molecular Dynamics Methods for Simulations in the Canonical Ensemble. Mol. Phys. 1984; 52:255–268.

[25]. Berendsen HJC, Grigera JR, Straatsma TP. The Missing Term in Effective Pair Potentials. J. Phys. Chem. 1987; 91:6269–6271.

[26]. Rick SW, Stuart SJ, Berne BJ. Dynamical Fluctuating Charge Force Fields: Application to Liquid Water. J. Chem. Phys. 1994; 101:6141–6156.

[27]. Bauer BA, Warren GL, Patel S. Incorporating Phase-Dependent Polarizability in Nonadditive Electrostatic Models for Molecular Dynamics Simulations of the Aqueous Liquid-Vapor Interface. J. Chem. Theory Comput. 2009; 5:359–373. [PubMed: 23133341]

[28]. Bauer BA, Patel S. Properties of Water Along the Liquid-Vapor Coexistence Curve via Molecular Dynamics Simulations Using the Polarizable TIP4P-QDP-LJ Water Model. J. Chem. Phys. 2009; 131:084709. [PubMed: 19725623]

[29]. Lamoureux G, Harder E, Vorobyov IV, Roux B, MacKerell AD Jr. Polarizable Model of Water for Molecular Dynamics Simulations of Biomolecules. Chem. Phys. Lett. 2006; 418:245–249.

[30]. Ryckaert JP, Ciccotti G, Berendsen HJC. Numerical Integration of the Cartesian Equations of Motion of a System with Constraints: Molecular Dynamics of *n*-Alkanes. J. Comp. Phys. 1977; 23:327–341.

[31]. Bauer BA, Patel S. Molecular Dynamics Simulations of Nonpolarizable Salt Solution Interfaces: NaCl, NaBr, and NaI in Transferable Intermolecular Potential 4-Point with Charge Dependent Polarizability TIP4P-QDP Water. J. Chem. Phys. 2010; 132:8107–8117.

[32]. Sanderson, RT. Chemical Bonds and Bond Energy. Academic Press; New York: 1976.

[33]. Rappe AK, Goddard WA. Charge Equilibration for Molecular Dynamics Simulations. J. Phys. Chem. 1991; 95:3358–3363.

[34]. Rick SW, Stuart SJ, Bader JS, Berne BJ. Fluctuating Charge Force Fields for Aqueous Solutions. J. Mol. Liq. 1995; 65/66:31.

[35]. Sanderson RT. An Interpretation of Bond Lengths and a Classification of Bonds. Science. 1951; 114:670–672. [PubMed: 17770191]

[36]. Warren GL, Davis JE, Patel S. Origin and Control of Superlinear Polarizability Scaling in Chemical Potential Equilization Methods. J. Chem. Phys. 2008; 128:144110. [PubMed: 18412426]

[37]. Lamoureux G, Roux B. Absolute Hydration Free Energy Scale for Alkali and Halide Ions Established from Simulations with a Polarizable Force Field. J. Phys. Chem. B. 2006; 110:3308–3322. [PubMed: 16494345]

[38]. Warren GL, Patel S. Hydration Free Energies of Monovalent Ions in Transferable Intermolecular Potential Four Point Fluctuating Charge Water: An Assessment of Simulation Methodology and Force Field Performance and Transferability. J. Chem. Phys. 2007; 127:064509. [PubMed: 17705614]

[39]. Warren GL, Patel S. Comparison of the Solvation Structure of Polarizable and Nonpolarizable Ions in Bulk Water and Near the Aqueous Liquid-Vapor Interface. J. Phys. Chem. C. 2008; 112:7455–7467.

[40]. Warren GL, Patel S. Electrostatic Properties of Aqueous Salt Solution Interfaces: A Comparsion of Polarizable and Nonpolarizable Ion Models. J. Phys. Chem. B. 2008; 112:11679–11693. [PubMed: 18712908]

[41]. Bauer BA, Ou S, Patel S. Role of Spatial Ionic Distribution on the Energetics of Hydrophobic Assembly and Properties of the Water/Hydrophobe Interface. Phys. Chem. Chem. Phys. 2012; 14:1892–1906. [PubMed: 22231014]

[42]. Bauer BA, Ou S, Patel S. Solvation Structure and Energetics of Single Ions at the Aqueous Liquid-Vapor Interface. Chem. Phys. Lett. 2011; 527:22–26. [PubMed: 23136448]

[43]. Fyta M, Kalcher I, Dzubiella J, Vrbka L, Netz RR. Ionic Force Field Optimization Based on Single-Ion and Ion-Pair Solvation Properties. J. Chem. Phys. 2010; 132:024911. [PubMed: 20095713]

[44]. Fyta M, Netz RR. Ionic Force Field Optimization Based on Single-Ion and Ion-Pair Solvation Properties: Going beyond Standard Mixing Rules. J. Chem. Phys. 2012; 136:124103. [PubMed: 22462831]

[45]. Wick CD, Lee AJ, Rick SW. How Intermolecular Charge Transfer Influences the Air-Water Interface. J. Chem. Phys. 2012; 137:154701. [PubMed: 23083178]

[46]. Lee AJ, Rick SW. The Effects of Charge Transfer on the Properties of Liquid Water. J. Chem. Phys. 2011; 134:184507. [PubMed: 21568521]

[47]. Darden T, York D, Pedersen L. Particle Mesh Ewald: An $N \cdot \log(N)$ Method for Ewald Sums in Large Systems. J. Chem. Phys. 1993; 98:10089–10092.

[48]. Yu H, Whitfield TW, Harder E, Lamoureux G, Vorobyov I, Anisimov VM, MacKerell AD Jr. Roux B. Simulating Monovalent and Divalent Ions in Aqueous Solution Using a Drude Polarizable Force Field. J. Chem. Theory Comput. 2010; 6:774–786. [PubMed: 20300554]

[49]. Miyamoto S, Kollman PA. Settle: An Analytical Version of the SHAKE and RATTLE Algorithm for Rigid Water Models. Journal of Computational Chemistry. 1992; 13:952–962.

[50]. Dang LX. Computational Study of Ion Binding to the Liquid Interface of Water. J. Phys. Chem. B. 2002; 106:10388–10394.

[51]. Wick CD, Dang LX. Recent Advances in Understanding Transfer Ions across Aqueous Interfaces. Chem. Phys. Lett. 2008; 458:1–5.

[52]. Dang LX, Chang TM. Molecular Mechanism of Ion Binding to the Liquid/Vapor Interface of Water. J. Phys. Chem. B. 2002; 106:235–238.

[53]. Wong K-Y, York DM. Exact Relation between Potential of Mean Force and Free-Energy Profile. J. Chem. Theory Comput. 2012; 8:3998–4003. [PubMed: 23185141]

[54]. Zhu F, Hummer G. Convergence and Error Estimation in Free Energy Calculations Using the Weighted Histogram Analysis Method. J. Comp. Chem. 2012; 33:453–465. [PubMed: 22109354]

[55]. Flyvbjerg H, Petersen HG. Error Estimates on Averages of Correlated Data. J. Chem. Phys. 1989; 91:461–466.

[56]. Pershan, PS.; Schlossman, M. Liquid Surfaces and Interfaces: Synchrotron X-ray Methods. Cambridge University Press; Cambridge: 2012. p. 4

[57]. Willard AP, Chandler D. Instantaneous Liquid Interfaces. J. Phys. Chem. B. 2010; 114:1954–1958. [PubMed: 20055377]

[58]. Ou S, Patel S. Temperature Dependence and Energetics of Single Ions at the Aqueous Liquid-Vapor Interface. J. Phys. Chem. B. 2013; 117:6512–6523. [PubMed: 23537166]

[59]. Kumar S, Bouzida D, Swendsen RH, Kollman PA, Rosenberg JM. The Weighted Histogram Analysis Method for Free-Energy Calculations on Biomolecules. I. The Method. J. Comp. Chem. 1992; 13:1011–1021.

[60]. Archontis G, Leontidis E, Andreou G. Attraction of iodide ions by free water surface, revealed by simulations with a polarizable force field based on Drude oscillators. J. Phys. Chem. B. 2005; 109:17957–17966. [PubMed: 16853305]

[61]. Horinek D, Herz A, Vrbka L, Sedlmeier F, Mamatkulov SI, Netz RR. Specific Ion Adsorption at the Air/Water Interface: The Role of Hydrophobic Solvation. Chem. Phys. Lett. 2009; 479:173–183.

[62]. Netz RR, Horinek D. Progress in Modeling of Ion Effects at the Vapor/Water Interface. Annu. Rev. Phys. Chem. 2012; 63:401–418. [PubMed: 22404593]

[63]. Baer MD, Mundy CJ. Toward an Understanding of the Specific Ion Effect Using Density Functional Theory. J. Phys. Chem. Lett. 2011; 2:1088–1093.

[64]. Stern AC, Baer MD, Mundy CJ, Tobias DJ. Thermodynamics of Iodide Adsorption at the Instantaneous Air-Water Interface. J. Chem. Phys. 2013; 138:114709. [PubMed: 23534655]

[65]. Godec A, Smith JC, Merzel F. Increase of Both Order and Disorder in the First Hydration Shell with Increasing Solute Polarity. Phys. Rev. Lett. 2011; 107:267801, 1–5. [PubMed: 22243182]

[66]. Lamoureux G, Roux B. Absolute Hydration Free Energy Scale for Alkali and Halide Ions Established from Simulations with a Polarizable Force Field. J. Phys. Chem. B. 2006; 110:3308–3323. [PubMed: 16494345]

[67]. Rahman A. Correlations in the Motion of Atoms in Liquid Argon. Phys. Rev. 1964; 136:A405–A411.

[68]. Choudhury N, Pettitt BM. Dynamics of Water Trapped between Hydrophobic Solutes. J. Phys. Chem. B. 2005; 109:6422–6429. [PubMed: 16851715]

[69]. Marti J, Nagy G, Guardia E, Gordillo MC. Molecular Dynamics Simulation of Liquid Water Confined inside Graphite Channels: Dielectric and Dynamical Properties. J. Phys. Chem. B. 2006; 110:23897–23994.

[70]. Jamadagni SN, Godawat R, Garde S. Hydrophobicity of Proteins and Interfaces: Insights from Density Fluctuations. Ann. Rev. Chem. Biomol. Eng. 2011; 2:147–171. [PubMed: 22432614]

[71]. Godec A, Merzel F. Physical Origin Underlying the Entropy Loss upon Hydrophobic Hydration. J. Am. Chem. Soc. 2012; 134:17574–17581. [PubMed: 23003674]

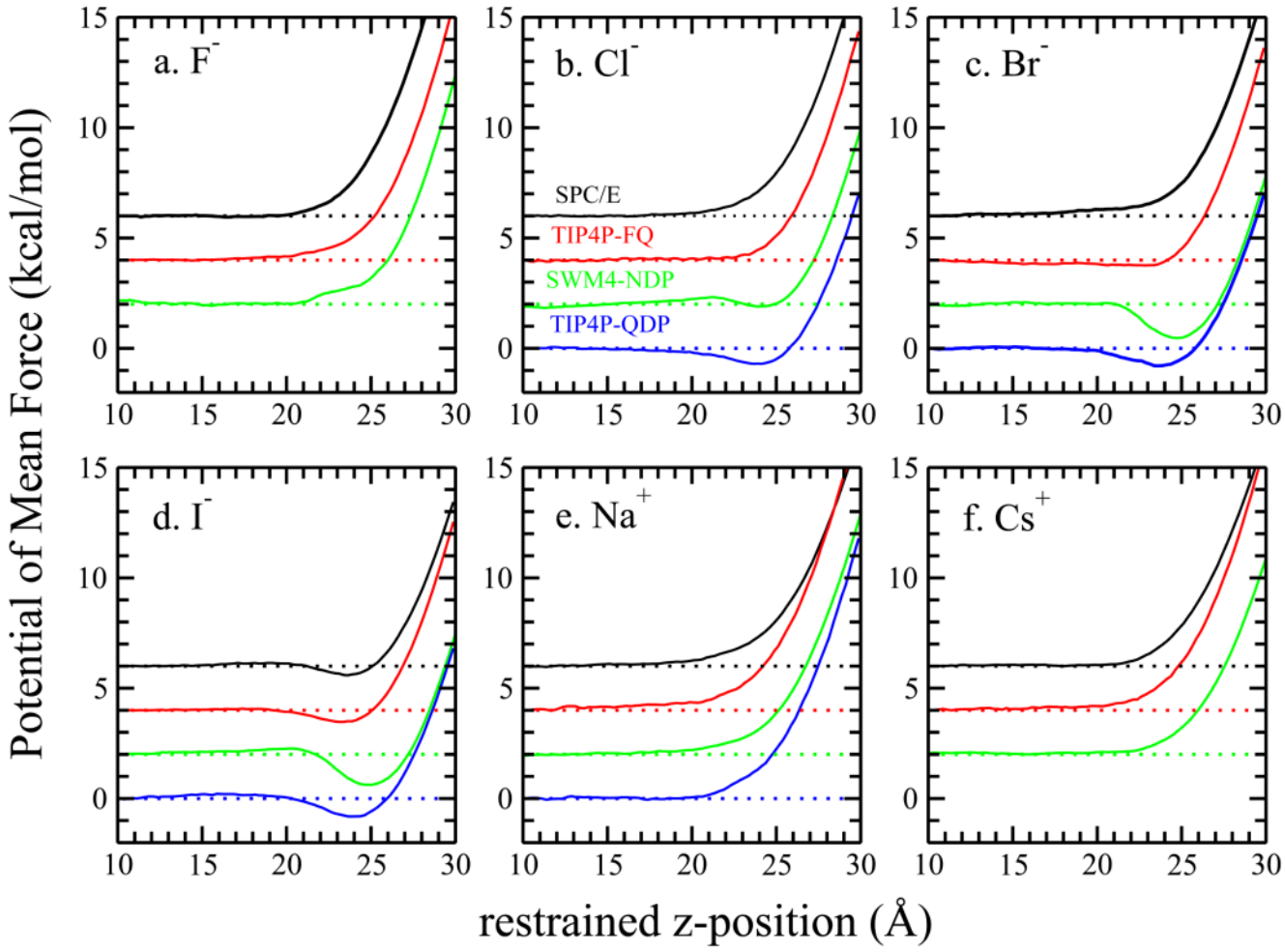

FIG. 1.

Potential of mean force for single ions transporting from bulk to vapor phase in different water force fields. A vertical off set of 2 kcal/mol is added for clarity.

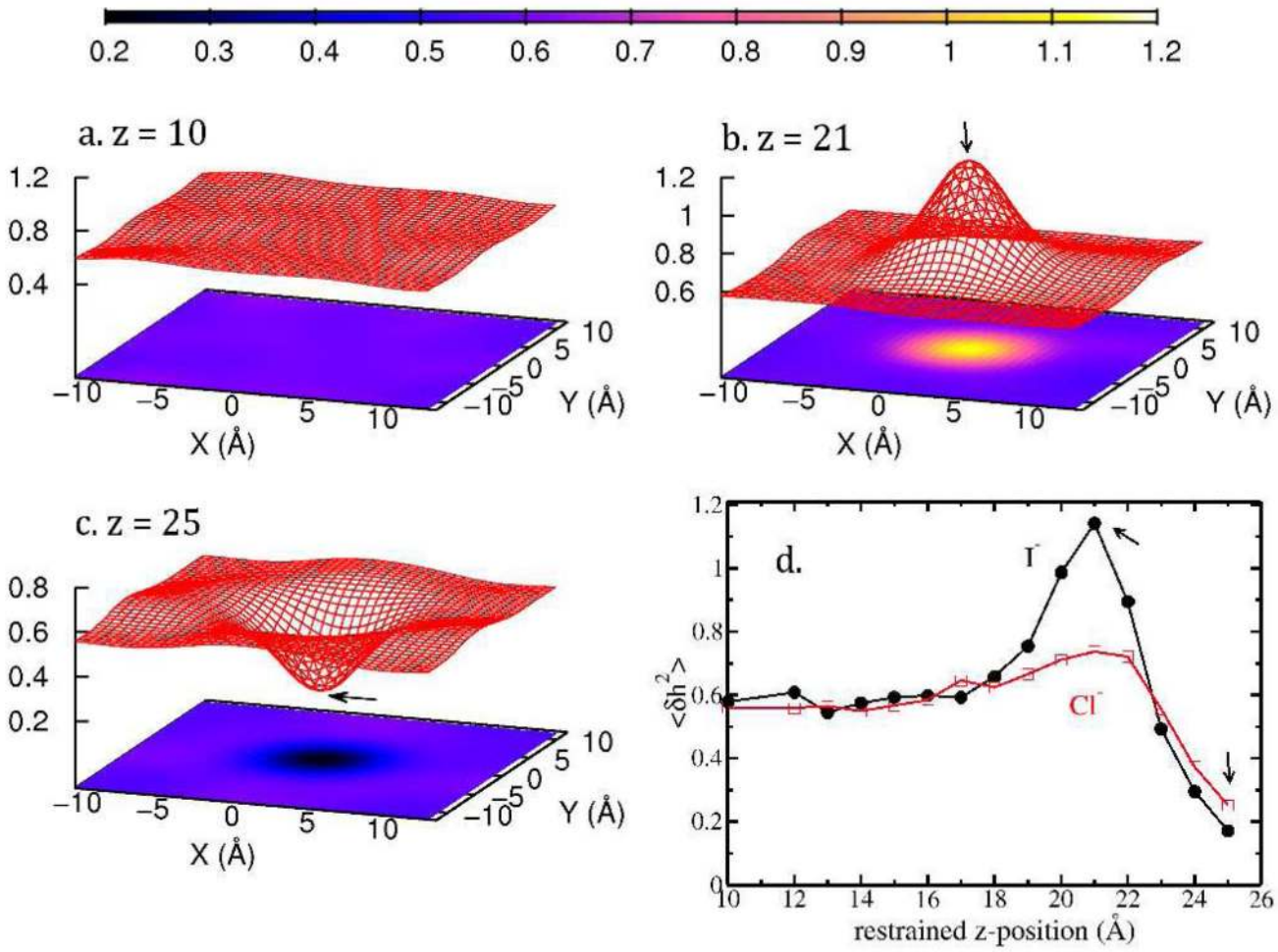

FIG. 2.

Average surface fluctuation $\langle \delta_{h2} \rangle$ for I^- in TIP4P-FQ, when the restrained position is at (a) z = 10 Å (b) z = 21 Å (c) z = 25 Å. Panel d shows the $\langle \delta h^2(x = 0, y = 0) \rangle$ (right above/below the ion, as indicated with arrows) as a function of ion restrained position for I^- and Cl^- in TIP4P-FQ.

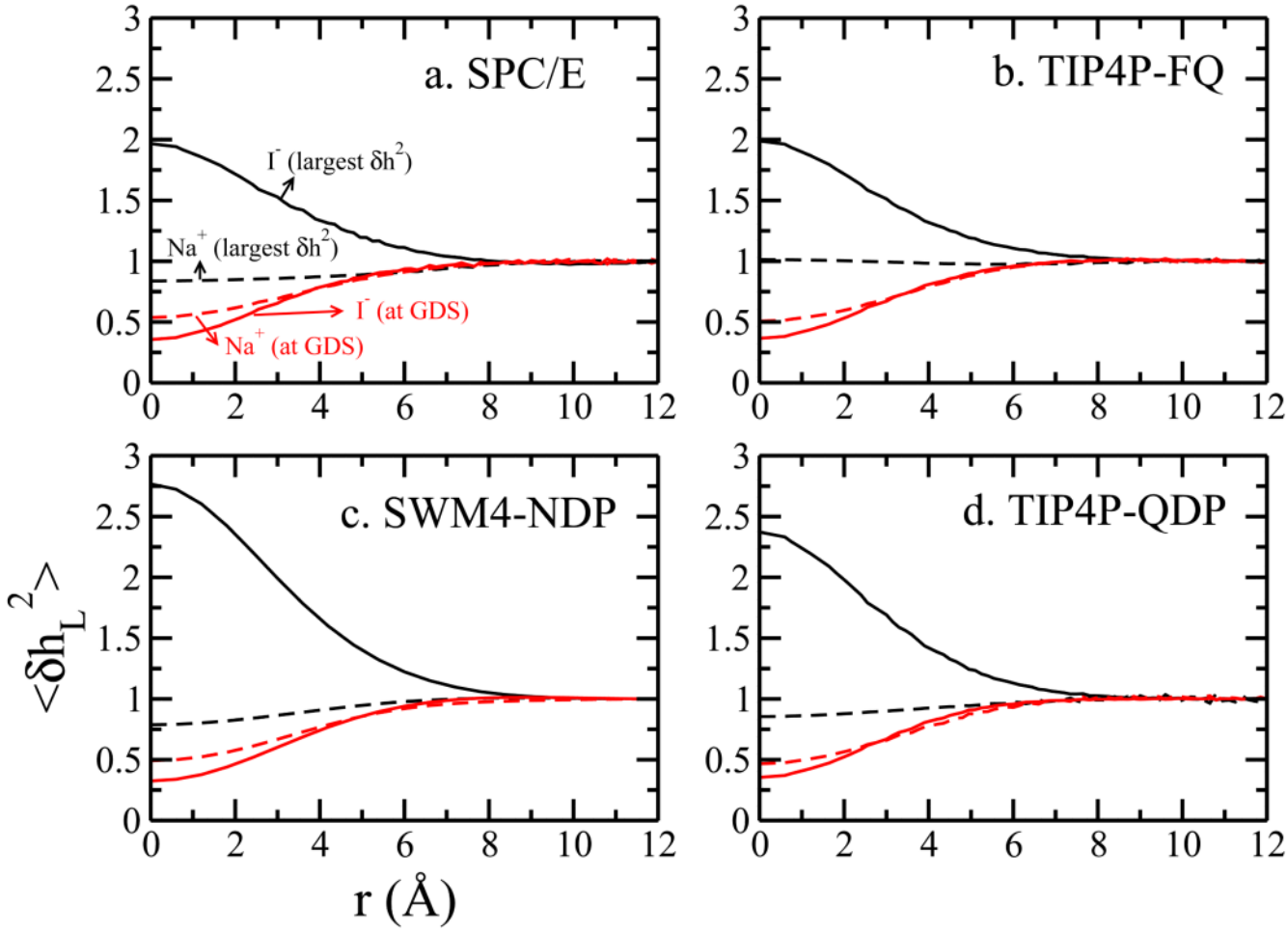

FIG. 3.

Normalized average surface fluctuation $\left\langle \delta h_{\mathrm{L}}^{2} \right\rangle$ as a function of radius from the I^{-}/Na^{+} in (a) SPC/E (b) TIP4P-FQ (c) SWM4-NDP (d) TIP4P-QDP force fields.

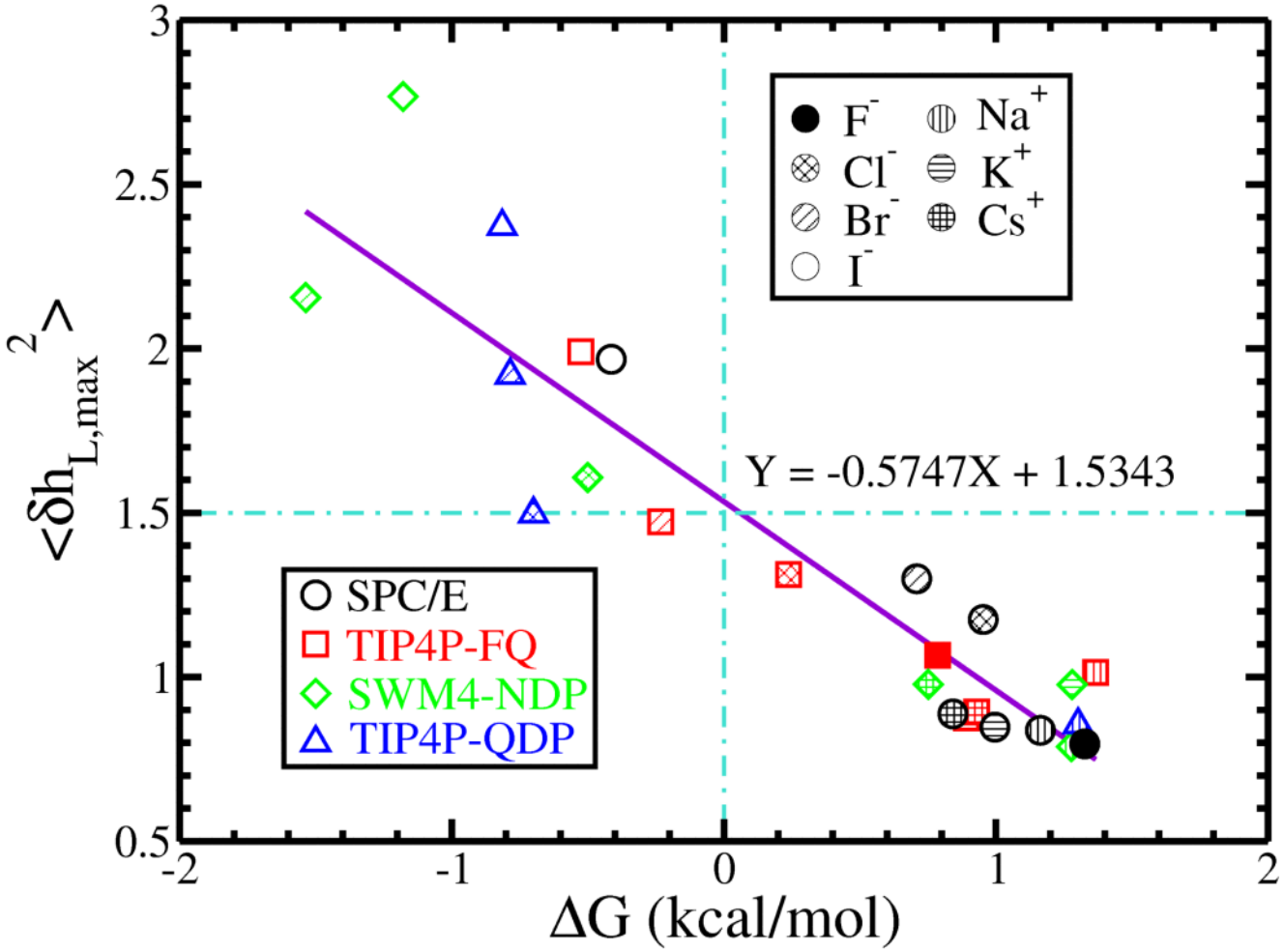

FIG. 4.

The largest normalized average surface fluctuation $\left\langle \delta h^2_{L,max} \right\rangle$ versus the corresponding free energy Δ*G* for ions in different force fields. All cations, which are not found to be surface stable in our work, are located in the lower right quadrant of the graph. All surface stable species (anions described by certain force fields) are found in the upper left quadrant.

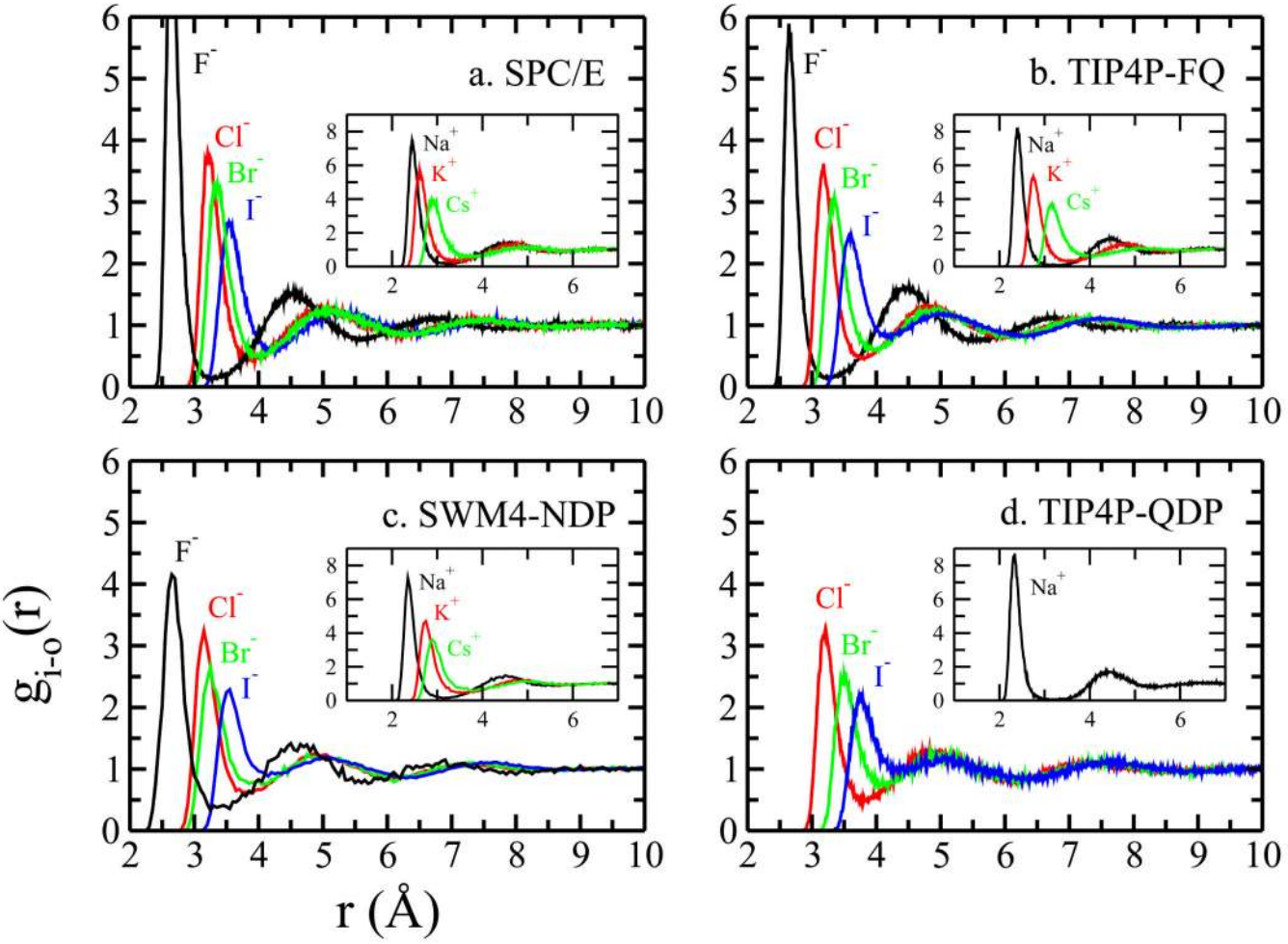

FIG. 5.

Ion-water radial distribution function (RDF) for anions in (a) SPC/E (b) TIP4P-FQ (c) SWM4-NDP (d) TIP4P-QDP force fields. The insets show the RDF of cations in the corresponding force field.

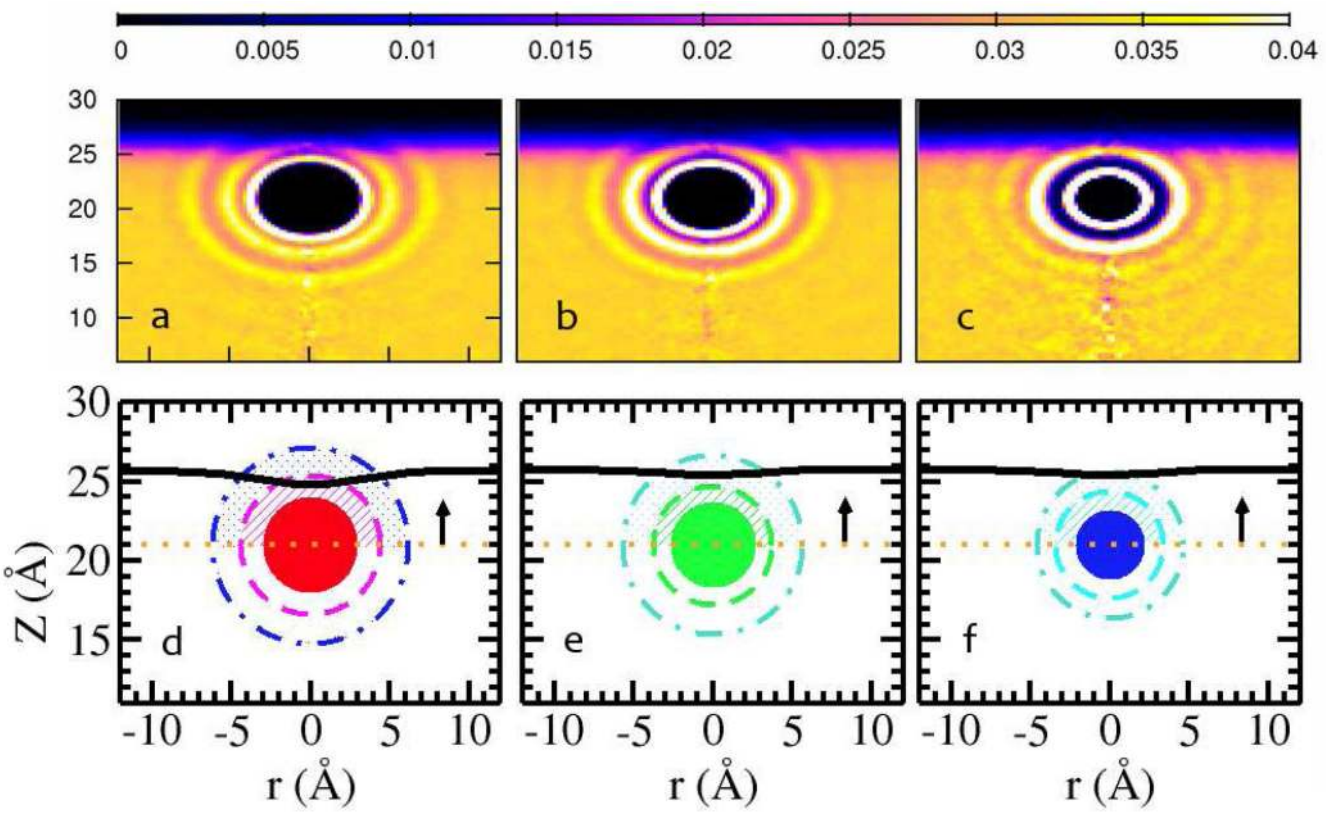

FIG. 6.

Average water oxygen density relative to (a) I^- (b) Cl^- (c) Na^+ at the position of 21.0 Å. (d)-(f) show the cartoon of ion with the cutoff of first solvation shell (dashed lines), second solvation shell (dot-dashed lines) and the calculated mean surface (solid black lines). For dynamical properties of water molecules in the shells of ions, we only study the water above the ion position (dotted lines).

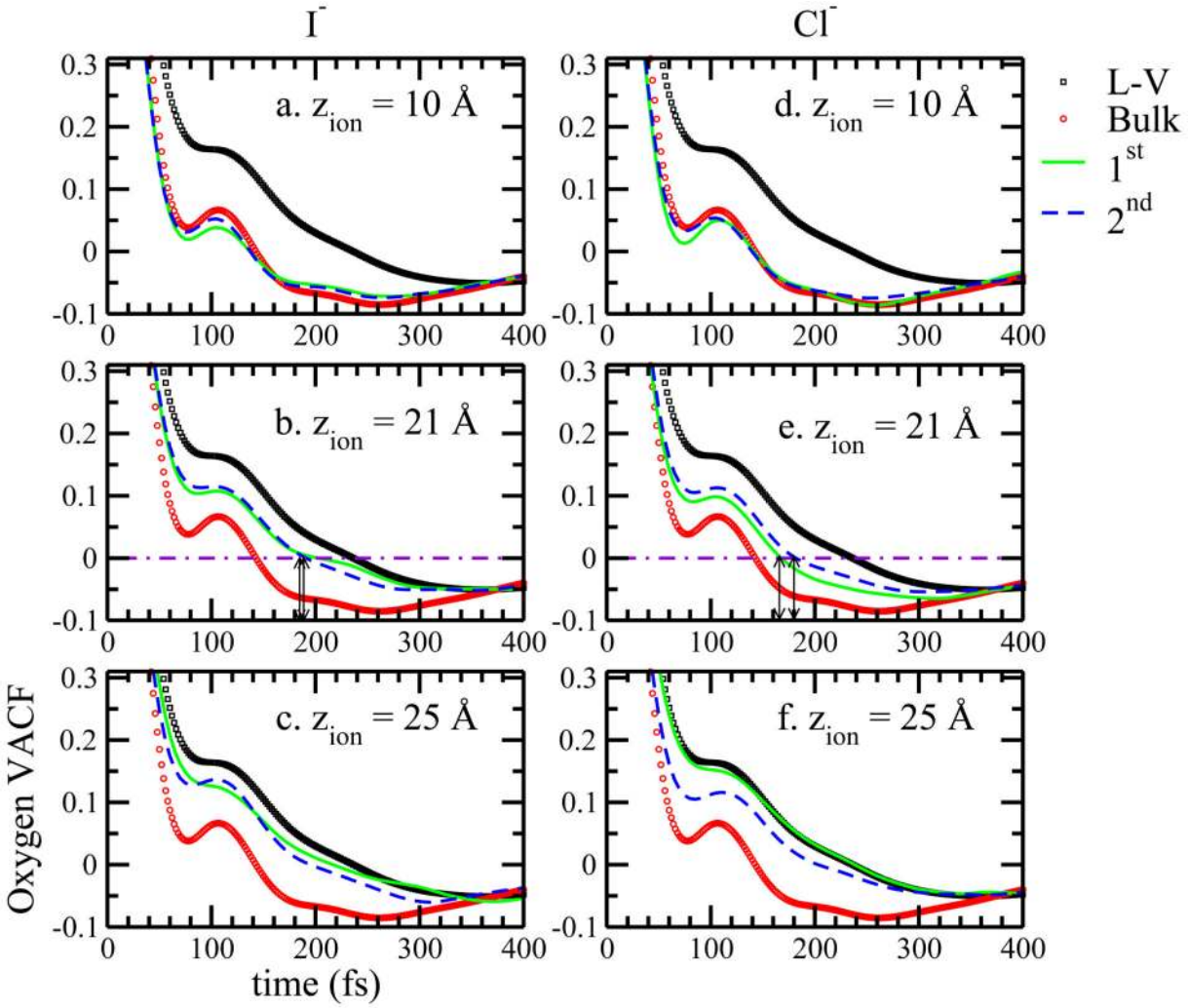

FIG. 7.

Oxygen velocity autocorrelation of water (TIP4P-FQ) in the bulk, near L-V interface, solvation shell water above I^-/Cl^-.

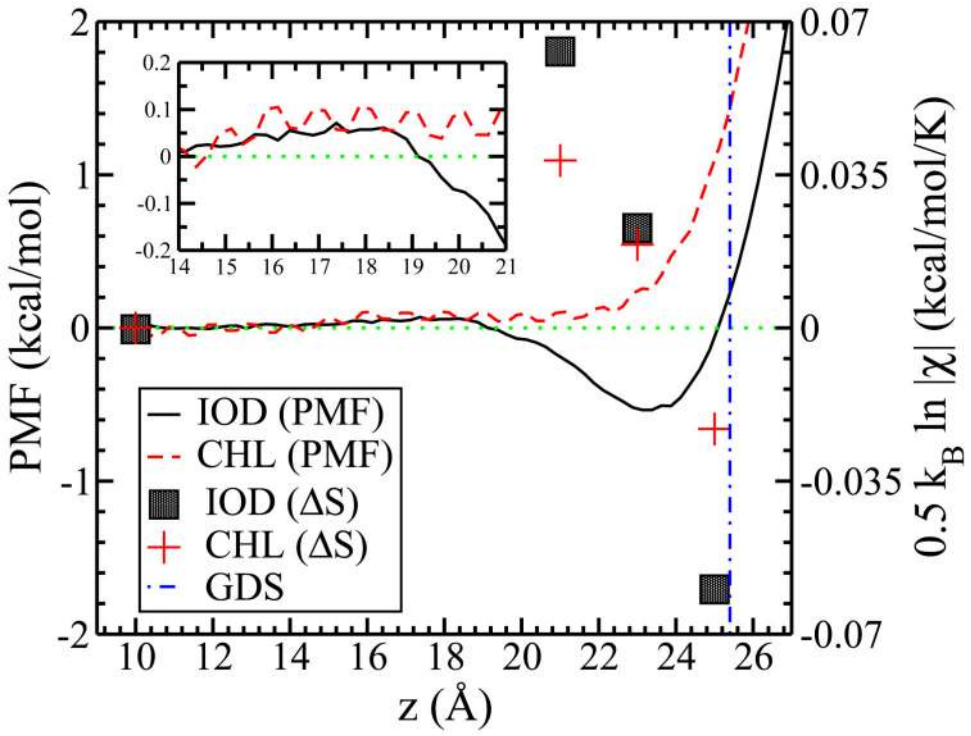

FIG. 8.

Potentials of mean force (PMF's) for I^- and Cl^- in TIP4P-FQ. Inset shows the region of ion positions from *z* = 14.0 to 21.0 Å. Symbols are semi-quantitative estimates of surface entropy (relative to bulk, hence Δ*S*) arising from ion-induced interfacial fluctuations using $S=constant+\frac{k_B}{2}ln|\mathscr{X}$ where $\mathscr{X}$ is the surface height function covariance matrix whose elements are $\mathscr{X}(\mathbf{r}_i,\mathbf{r}_j)=\langle\delta h(\mathbf{r}_i)\,\delta h(\mathbf{r}_j)\rangle$. Finally, $\delta h(\mathbf{r}_i) = h(\mathbf{r}_i) - \langle h(\mathbf{r}_i)i\rangle$.

TABLE I

Parameters of water models used in this study.

	R_{min} (Å)	ε (kcal/mol)
SPC/E	3.5532	0.1554
TIP4P-FQ	3.5459	0.2862
SWM4-NDP	3.5698	0.2057
TIP4P-QDP	3.5520	0.2902

TABLE II

Parameters of ions used in this study. Uncertainty in the last digit denoted in parentheses.

	R_{min} (Å)	ε (kcal/mol)	ΔG_{hyd} (kcal/mol)
SPC/E			
F^-	4.6706	0.003585	−102.77
Cl^-	4.9388	0.1	−73.14
Br^-	5.1981	0.09847	−66.68
I^-	6.5451	0.003085	−57.60
Na^+	2.8993	0.1	−98.95
K^+	3.0194	0.5832	−82.22
Cs^+	3.9185	0.07768	−71.22
TIP4P-FQ			
F^-	4.52	0.01	−112.83(9)
Cl^-	4.92	0.07658	−78.93(8)
Br^-	5.14	0.10820	−71.87(14)
I^-	5.52	0.15910	−63.15(15)
Na^+	2.90	0.03151	−98.41(12)
K^+	3.29	0.18290	−82.05(10)
Cs^+	3.96	0.35279	−69.63(8)
SWM4-NDP			
F^-	4.9245	0.002618	−108.0
Cl^-	4.9622	0.07197	−78.4
Br^-	5.2526	0.0823	−71.6
I^-	5.5159	0.2084	−63.1
Na^+	2.9234	0.0315	−96.3
K^+	3.3733	0.1419	−78.6
TIP4P-QDP			
Cl^-	5.6419	0.01142	−74.4(2)
Br^-	5.6839	0.05740	−63.1(7)
I^-	5.8339	0.1569	−57.5(1)
Na^+	2.6939	0.031075	−103.2(1)

TABLE III

Fitting results of residence time of water molecules in the first solvation shell. Values in parentheses denote the uncertainty determined from the standard deviation.

System	τ (ps)	γ
I^-, TIP4P-FQ, 10.0 Å	1.62(0.28)	0.78(0.04)
I^-, TIP4P-FQ, 21.0 Å	1.12(0.25)	0.80(0.05)
I^-, TIP4P-FQ, 25.0 Å	1.47(0.13)	0.86(0.08)
Cl^-, TIP4P-FQ, 10.0 Å	2.57(0.22)	0.84(0.04)
Cl^-, TIP4P-FQ, 21.0 Å	2.74(0.08)	0.86(0.09)
Cl^-, TIP4P-FQ, 25.0 Å	2.46(0.08)	0.85(0.16)
I^-, SWM4-NDP, 10.0 Å	1.82(0.94)	0.76(0.14)
I^-, SWM4-NDP, 21.0 Å	1.27(0.86)	0.72(0.12)
I^-, SWM4-NDP, 25.0 Å	0.83(0.67)	1.04(0.25)
Cl^-, SWM4-NDP, 10.0 Å	3.38(1.91)	0.88(0.15)
Cl^-, SWM4-NDP, 21.0 Å	2.00(0.82)	0.91(0.10)
Cl^-, SWM4-NDP, 25.0 Å	2.41(2.33)	1.04(0.25)